Optoelectronic Materials ISSN 2377-4738 *Optoelectron. Mater. 2 (2017) 1–7*

Low power conversion efficiency of silicon quantum dots sensitized solar cells

Chen Tang, Bao-gai Zhai, Yuan Ming Huang*

School of Mathematics and Physics, Changzhou University, Jiangsu 213164, China

(*Received 9 January 2017; accepted 5 February 2017*)

Si quantum dots sensitized solar cells (QDSSCs) were prepared by using Si quantum dots as the sensitizer, porous TiO_2 thin film as the photoanode, and polysulfide as the electrolyte. The surface morphology, crystal structure and optical properties of the photoanode and Si quantum dots were characterized by the scanning electron microscope, transmission electron microscope, X-ray diffractometer and photoluminescence spectrophotometer, respectively. The photocurrent density–photovoltage characteristics were recorded for the Si QDSSCs by a solar cell measurement system. The results indicate that the power conversion efficiency of Si QDSSCs is as low as 0.052%. One possible reason for the low power conversion efficiency is the formation of SiO_2 insulating layer on the surface of Si quantum dots. Our results suggest that Si quantum dots are not suitable sensitizer for QDSSCs. New kinds of quantum dots are required to promote QDSSCs with a promising future.

Keywords: Quantum dots sensitized solar cell; Si quantum dot; Power conversion efficiency

1. Introduction

The emergence of global warming due to excessive use of fossil fuels has led us to focus on renewable and clean energy sources. Photovoltaic cell, which is an electrical device that converts the energy of light directly into electricity by the photovoltaic effect, is proposed to be the ideal solution to the problem of global warming. As discussed in the literature, photovoltaic cells can be classified into three generations [1]. The first generation solar cells are based on single or polycrystalline *p–n* junction silicon cells. They are the most common photovoltaic converters, these cells have a current market share of approximately 85%, and silicon based photovoltaic devices have reached the power conversion efficiency of about 25%. However, high purity requirements for silicon crystals, high fabrication temperatures, high material cost, and negative environmental impact of the processing technologies are major problems that should be resolved. The second generation photovoltaic devices are based on inorganic thin films, they have a current market share of approximately 15%. These devices are mostly based on CdTe. The second generation photovoltaic devices are cheaper but are less efficient than the first generation single-junction crystalline photovoltaic cells. Thus, for further improvement, new technologies are required to produce the third generation solar cells with an efficiency of more than 33% but has lower production cost.

Dye sensitized solar cells (DSSCs), which are a member of the third generation solar cells, are considered low-cost and high-efficiency solar cells because their manufacture requires low cost materials and simple processes with added functionalities such as low weight, flexibility, and semi-transparency [2]. Extensive efforts have been exerted to increase the efficiency of DSSCs, however, the development of DSSCs has contributed to no more than 12% of the highest recorded efficiency over the last 10 years [3-7]. In order to find solutions to this deadlock, quantum dots with tunable band gaps are explored to replace the organic dyes of ruthenium polypyridine complexes in DSSCs in the hope of enhanced efficiency due to the advantages of broadened photo response in the solar spectrum. The size quantization of a quantum dot allows for the band gap to be tuned by simply changing particle size. Thus the quantum dots of inorganic semiconductors can serve as dye replacements for next generation sensitizers, and quantum dots solar cells (QDSSCs) are intensively studied since 2005 [8-11]. In a QDSSC, a mesoporous layer of titanium dioxide (TiO_2) nanoparticles forms the backbone of the cell, much like in a DSSC. This TiO_2 layer can then be made photoactive by coating with semiconductor quantum dots using chemical bath deposition, electrophoretic deposition or successive ionic layer adsorption and reaction. The electrical circuit is then completed through the use of a liquid or solid redox couple.

Quantum dots sensitized solar cells (QDSSCs) are based on the DSSC architecture but employ low band gap semiconductor nanoparticles. Up to date, a variety of quantum dots such as CdS, CdSe, CdTe and PbS are employed as the light absorbers in QDSSCs [8-11]. Among them, Cd compound-based sensitized solar cells display the highest conversion efficiency at present so that most researches are concentrating on them. The efficiency of QDSSCs has increased to over 5% shown for both liquid-junction and solid state cells. However cadmium is highly toxic and tellurium supplies are limited. The cadmium present in the cells would be toxic if released. Therefore, it is important to develop non-toxic and abundant quantum dots for QDSSCs for efficient light harvesting.

Si quantum dot is one of the outstanding quantum dot materials and it exhibits the advantages of abundance and non-toxicity that make Si become the backbone of the electronics and solar cell industry. The fascinating advantages of Si quantum dots include: (i) non-toxicity and abundance in nature, (ii) simplicity and low cost for large scale production, (iii) high extinction coefficient and tunable band gap by size controlling [12-15]. Thus Si quantum dots are promising candidate that is expected to open an alternative path for harvesting light energy from visible to infrared regions of the solar spectrum. Moreover, two research groups explored Si quantum dots

*Corresponding author. Email: dongshanisland@126.com

in fabricating QDSSCs. They prepared Si quantum dots by multi-hollow discharge plasma chemical vapor deposition, and polysulfide electrolyte were generally used because it was suitable for stabilizing Si quantum dots and its redox reaction was the best as compared with other redox systems [16-22]. Despite the good characteristics of Si quantum dot, it is found that the power conversion efficiency of Si QDSSCs is as low as 0.02%, which is much lower than that of the conventional QDSSCs (5%). One of the primary reasons can be attributed to the poor combination between Si quantum dots and TiO_2 porous film. Very a few of Si quantum dots adsorption on the TiO_2 surface will not only cause too low photocurrent of Si quantum dots, but also increase the charge recombination at TiO_2/electrolyte interface, which leads to the decrease of photovoltage and fill factor. In order to overcome this difficulty and improve the overall performance of Si QDSSCs, Seo et al built the bonding between Si quantum dots and TiO_2 porous film by functionalization of Si quantum dots using 4-vinylbenzoic acid as the linking source [21]. Consequently, more Si quantum dots adsorbed on the surface of TiO_2 porous film and the contact area between TiO_2 and electrolyte was reduced, thus enhancing the photocurrent and reducing the charge recombination of Si QDSSCs.

In this paper we reported the photovoltaic performance of Si QDSSCs. The Si quantum dots were made by etching single crystalline Si substrate in hydrofluoric acid. Our results demonstrated that the Si QDSSCs exhibited quite low efficiency (0.056%). Although Si quantum dots are the most applicable material for photo sensitization because of their high absorption and the size tunable emission spectrum, our results demonstrated that Si quantum dots are not suitable sensitizer for QDSSCs.

2. Materials and method

2.1. Reagents and materials

Tetrabutyl titanate, acetate acid, polyethylene glycol (PEG-2000), chloroplatinic acid hexahydrate ($H_2PtCl_6 \cdot 6H_2O$), sublimed sulfur (S), methanol, ethanol and acetone were purchased from Sinopharm Chemical Reagent Co., Ltd. Titanium tetrachloride ($TiCl_4$), butyl alcohol, diethanolamine and potassium chloride (KCl) were supplied by Shanghai Lingfeng Chemical Reagent Co., Ltd. Sodium sulfide nonahydrate ($Na2_S \cdot 9H_2O$) was purchased from Wuxi Yasheng Chemical Co., Ltd. Fluorine-doped tin oxide conductive glass (FTO, sheet resistance ~14 Ω /cm^2, thickness 2.2 mm) and thermoplastic hot-melt sealant (Surlyn 1702, thickness 25 μm) were provided by Wuhan Geao Co., Ltd. All reagents were used as received without further purification.

2.2. Synthesis of porous Si film and Si quantum dots

The porous Si film was synthesized by electrochemical anodization of boron doped p-type (111)-oriented Si wafer in hydrofluoric electrolyte [12-14, 23-25]. The resistivity of Si wafer was in the range of 8-13 Ω • cm. The electrolyte was an equal volume mixture of hydrofluoric acid (40 wt%) and ethanol (98 wt%). A platinum wire was utilized as the counter electrode while the Si wafer was employed as the working electrode. The anodizing current density was fixed to be 10 mA/cm^2 and the anodization duration was 30 min. The porous Si film was rinsed in ethanol repeatedly and dried in the oven. Afterwards, the Si nanoparticles were scraped from porous Si film to the beaker using a doctor blade followed by adding moderate amounts of ethanol. The Si nanoparticles were dispersed uniformly in ethanol by ultrasonic treatment to obtain an ethanolic suspension solution of Si quantum dots.

2.3. Preparation and decoration of TiO_2 porous film

The FTO substrate (2.5 × 2.0 cm) was sequentially cleaned in detergent, deionized water, acetone and ethanol with the assistance of ultrasonic treatment. After dried in the oven, the FTO substrate was immersed in an aqueous solution of $TiCl_4$ (0.04 M) at 70°C for 30 min and then sintered at 450°C for 30 min to form a TiO_2 compact layer. Subsequently, the TiO_2 porous film was prepared by a sol-gel process. In brief, the $TiCl_4$ coated FTO substrate was dipped into the TiO_2 sol for about 1 min, pulled out and dried in the oven. This dipping-pulling-drying process was repeated 8 times to guarantee the thickness of TiO_2 porous film. The TiO_2 sol was synthesized by adding 4 mL of tetrabutyl titanate, 2 mL of diethanolamine, 1.5 mL of deionized water, 1.2 mL of acetate acid and 0.045 g of PEG-2000 into 60 mL of butyl alcohol under stirring at room temperature and aged for about 16 h. Finally, the TiO_2 sol coated FTO substrate was calcined at 450°C for 2 h to form porous TiO_2 film. For the surface decoration of TiO_2 porous film, a small amount of TiO_2 sol was directly dropped on the as-prepared TiO_2 porous film. After dried in the air, the TiO_2 film was sintered again at 450°C for 30 min to increase the crystallinity of TiO_2 film.

2.4. Assembling of QDSSC

Si QDSSC was assembled by the following procedure. Several drops of the ethanolic suspension solution of Si quantum dots were dropped onto TiO_2 film. After drying in air, Si quantum dots sensitized TiO_2 thin film was ready for the photo electrode. The platinum counter electrode was prepared by immersing a clean FTO substrate into the ethanolic solution of H_2PtCl_6 (4 mM), drying the substrate in the oven and then sintering the substrate at 450°C for 2 h. The photo electrode and counter electrode were assembled into a sandwich structure using a Surlyn film. The internal space between two electrodes was filled with a redox electrolyte through the pre-drilled hole on the counter electrode. Polysulfide electrolyte is suitable as the redox couple in case of QDSSC because quantum dots are degraded by I^-/I_3^- electrolyte. The redox electrolyte consisted of 0.5 M Na_2S, 2 M S and 0.2 M KCl in the mixture of methanol and deionized water at a volume ratio of 7:3. Finally, the hole on the counter electrode was sealed by a Surlyn film and a cover glass.

2.5. Characterizations

A field emission scanning electron microscope (SEM, S-4800, Hitachi, Japan) was utilized to characterize the surface morphology of TiO_2 porous film. The particle size of Si quantum dots was observed by a transmission electron microscope (TEM, JEM-2100, JEOL), operating

at an accelerating voltage of 200 KV. The crystalline structure of sample was analyzed by X-ray diffractometer (XRD, D/max 2500 PC, Rigaku, Japan) with a Cu K α radiation (λ = 0.15406 nm). The photoluminescence (PL) spectrum of sample was recorded with a spectrophotometer and the 325 nm laser line from a He-Cd laser was employed as the excitation source. For the photovoltaic performance measurement of Si QDSSC, an AM 1.5 solar simulator with a 500 W xenon lamp was used to illuminate the fabricated QDSSC and the incident light power was calibrated to 100 mW/cm^2. The photocurrent density (J) and photovoltage (V) of QDSSC were recorded with a Keithley model 2400 digital source meter.

3. Results and discussions

3.1. Crystal structure and morphology

The crystal structures of Si quantum dot sensitized TiO_2 film are analyzed with XRD. Fig. 1 shows the XRD spectra of Si quantum dots sensitized TiO_2 thin film (*a*), anatase titania (PDF#21-1272) (*b*) and crystalline Si (PDF#27-1402) (*c*). As seen in Fig. 1(a), the diffraction peaks at 2 θ = 25.3°, 37.8°, 48.0°, 55.1°, 62.7° and 75.0° (marked with blue squares) can be assigned to the reflections from (101), (004), (200), (211), (204) and (215) crystallographic planes of anatase TiO_2, according to the

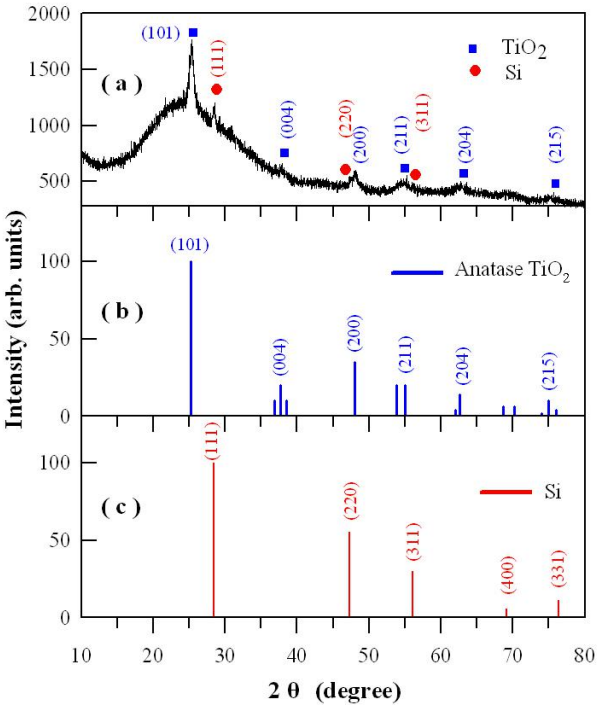

Fig. 1 XRD spectra of Si quantum dots sensitized TiO_2 thin film (*a*), anatase titania (PDF#21-1272) (*b*) and crystalline Si (PDF#27-1402) (*c*).

Joint Committee on Powder Diffraction Standard (JCPDS No. 21-1272). This verifies that the anatase TiO_2 is formed using the sol-gel method. Additionally, three diffraction peaks are observed in Fig. 1(a), they are located at 2 θ = 28.4°, 47.3° and 56.1° (marked with red circles), corresponding to the reflections from the (111), (220) and (311) crystallographic planes of cubic Si (JCPDS No. 27-1402). Thus Fig. 1(a) gives evidence that Si quantum dots are present in the TiO_2 porous film. It is worth noting that a broad diffraction band centered at about 22° appears in the XRD spectrum of Si quantum dots sensitized TiO_2 thin film, as shown in Fig. 1(a). Such a broadband diffraction suggests the presence of some kind of amorphous material in the photoanode. After having separately measured the XRD spectra of TiO_2 thin film and Si quantum dots, we found the amorphous band comes from Si quantum dots. It is known that Si quantum dots can be easily oxidized in air [24]. Consequently, Fig. 1(a) shows that the Si quantum dots in the TiO_2 film are partially oxidized.

Fig. 2 shows the SEM micrographs of the TiO_2 porous film before (a) and after (b) Si quantum dots sensitization. As shown in Fig. 2 (a), the TiO_2 porous film prepared via the sol-gel method is composed of a large quantity of TiO_2 nanoparticles. There are plentiful of nanopores in the TiO_2 thin film, and the size of nanopores is too small to be discernible when characterized with a SEM. After coated with a few drops of TiO_2 sol, the surface of TiO_2 porous film is changed markedly with the appearance of many large grooves on the film surface. Additionally, it is found that a lot of large Si spheres with the size of about 200-300 nm in diameter are caught in the grooves. According to quantum theory, quantum confinement effect becomes invalid for these large Si nanoparticles [12-14].

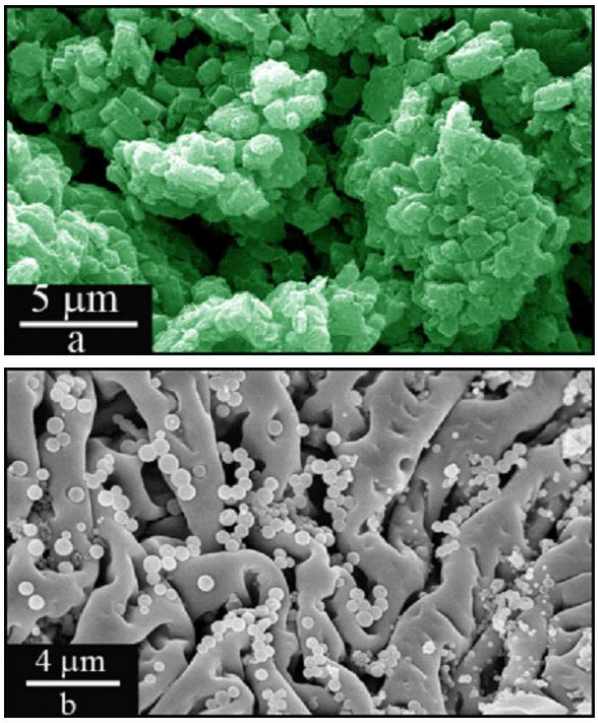

Fig. 2 SEM micrographs of TiO_2 porous film before (*a*) and after (*b*) the Si quantum dots sensitization.

Further investigation on the actual size of Si quantum dots is performed with the TEM measurement. Fig. 3 illustrates the low resolution TEM micrograph (*a*), the high resolution TEM micrograph (*b*) and the selected area electron diffraction pattern (*c*) of Si quantum dots in the Si quantum dots sensitized TiO_2 photoanode. As displayed in Fig. 3 (a), the as-prepared Si quantum dots

from porous Si film are nanoparticles whose typical size is about 10 nm. One possible reason for the large size of Si quantum dots observed in Fig. 2 (b) may be that Si quantum dots have agglomerated together when they are coated onto the TiO_2 film surface. On the other hand, the high-resolution TEM image in Fig. 3 (b) indicates that the spacing between two adjacent planes of Si quantum dots is 0.3135 nm, which is consistent with the standard spacing of two (111) planes in the cubic Si crystal. The micrograph in Fig. 3(b) suggests that the Si quantum dot, except the outer surface layer, is crystalline in nature. Fig. 3 (c) depicts the selected area electron diffraction pattern of Si quantum dots and it further confirms the crystalline nature of Si quantum dots because of the presence of diffraction spots in the selected area electron diffraction pattern.

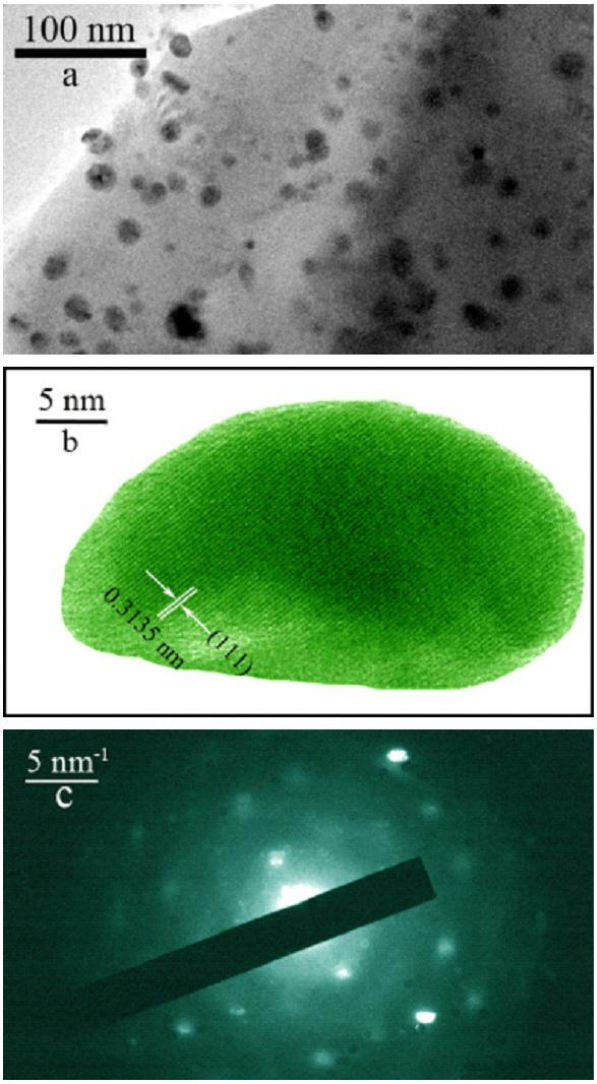

Fig. 3 TEM images of Si quantum dots prepared from the porous Si film: (*a*) low resolution, (*b*) high resolution, (*c*) selected area electron diffraction pattern.

3.2. PL spectrum of Si quantum dots sensitized TiO_2 photoanode

Fig. 4 illustrates the room-temperature PL spectra of the TiO_2 porous film (*a*) and the Si quantum dots sensitized TiO_2 photoanode (*b*). It is apparent that the peak of the PL spectra of TiO_2 thin film is located at at 410 nm, as shown in Fig. 4(a). It is generally believed that the PL emissions of anatase TiO_2 can be attributed to self-trapped excitons, surface states and oxygen vacancies [3,7]. So the PL band in Fig. 4(a) is attributed to the oxygen vacancies in the TiO_2 porous film [3,7]. The PL spectrum in Fig. 4 (b) can be decomposed into a relatively weak violet PL band centered at about 410 nm and a relatively strong red PL band centered at about 608 nm. The comparison of the PL spectra in Fig. 4 indicates that the PL band peaking at 410 nm belongs to TiO_2 porous film while the red PL band centered at 608 nm originates from Si quantum dots [24-26].

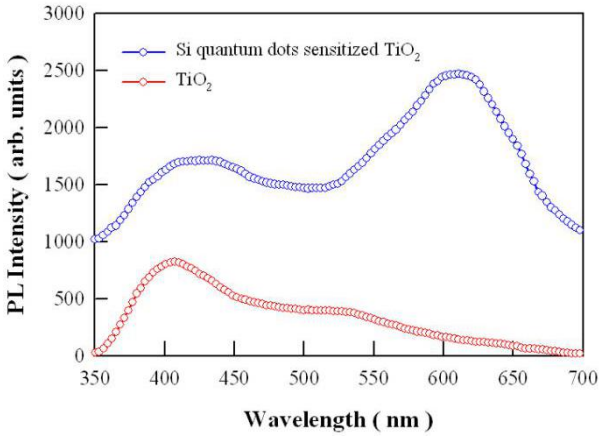

Fig. 4 PL spectra of TiO_2 porous film (*a*) and Si quantum dots sensitized TiO_2 film (*b*).

3.3. Photovoltaic performance of Si QDSSCs

Fig. 5 presents the *J-V* characteristic curves of two Si QDSSCs under a light illumination intensity of 100 mW/cm^2. On the basis of *J-V* curve *a*, the short circuit current density, open circuit voltage, filling factor and power conversion efficiency of the first Si QDSSC are 0.253 mA/cm^2, 0.400 V, 0.316 and 0.032%, respectively. As a contrast, J-V curve *b* shows that the short circuit current density, open circuit voltage, filling factor and power conversion efficiency of the second Si QDSSC are 0.428 mA/cm^2, 0.402 V, 0.302 and 0.052%, respectively. Apparently, the power conversion efficiency of the Si QDSSCs varies from one cell to the other cell. Moreover, we measured the *J-V* curve of one solar cell without the sensitizer, i.e., the Si quantum dots. It was found that both the photocurrent density and the open circuit voltage of the solar cell can be neglected when compared to the two *J-V* curves in Fig. 5. Consequently we can conclude that the photocurrent in Fig. 5 results from Si quantum dots sensitization of the TiO_2 film. This result implies that Si quantum dots can absorb the photons under light irradiation, and the electrons in valence band of Si quantum dots are excited to conduction band and then flow to the outer circuit as photocurrent. But it can be seen clearly that the power conversion efficiency of the Si QDSSCs is very low when compared to the current record for QDSSCs (i.e., 5%).

DSSCs consist of a dye-sensitized photoanode, a counter electrode, and an electrolyte (mostly iodide). The photoanode is composed of an oxide semiconductor material, particularly TiO_2, which is a highly stable electron collector under visible light illumination. The

resultant film is normally 10 mm thick and exhibits a nanoporous structure that increases dye absorbance on the TiO_2 film. The dye sensitizer (a Ru complex) is subsequently absorbed onto the TiO_2 surface, which leads to photon absorption and electron injection. The electrolyte I^-/I_3^- is frequently used to transfer electrons between TiO_2 and the counter electrode. Tri-iodide ions, which are created by the reduction of dye cations with the I^- ion, are then reduced to I_3^- ions at the counter electrode. Pt- and carbon-based materials coated on the FTO substrate are generally used as counter electrodes. The physically blocked FTO–electrolyte interface effectively prevents the injected electrons in the FTO to recombine with the redox in the electrolyte.

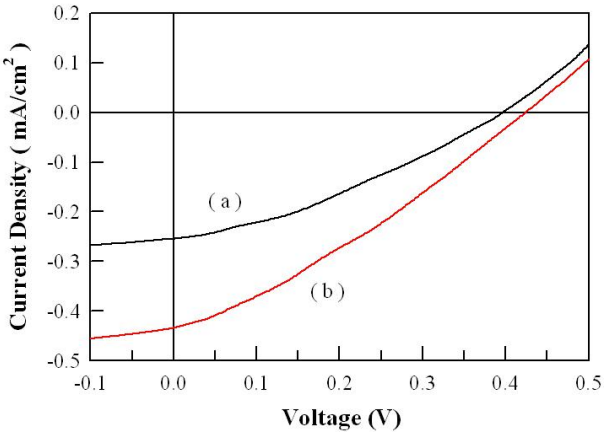

Fig. 5 *J-V* characteristic curves of two Si QDSSCs.

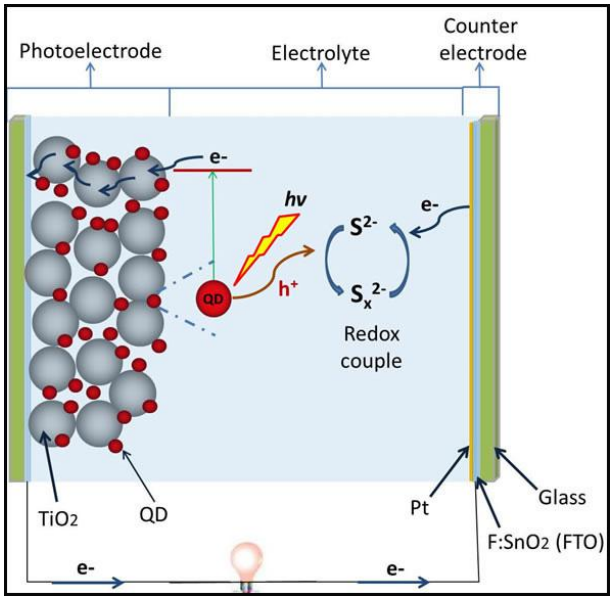

Fig. 6 *J-V* characteristic curves of two Si QDSSCs.

The only difference between DSSCs and QDSSCs is the sensitizing material that is substituted by inorganic nanoparticle quantum dots in the case of QDSSCs. Fig. 6 shows the operating principle of a typical QDSSC. Electron–hole pairs are created in the quantum dots as they progress from the lower valence band to the excited state (i.e., the conduction band). Electrons from the conduction band of quantum dots are injected into that of TiO_2 upon illumination, resulting in the oxidation of the photosensitizer. The ground state of quantum dots is regenerated through electron donation from the electrolyte, which is commonly a redox system such as polysulfide (S^{2-}/S_x^{2-}) redox couples. Another oxidation then occurs in the photoanode–electrolyte interface in the electrolyte

$$S^{2-} + 2h \rightarrow S \quad (1)$$

and

$$S + S_{x-1}^{2-} \rightarrow S_x^{2-} (x = 2-5) \quad (2)$$

On the counter electrode, the oxidized groups S2-x are reduced to S2-. Hence, electrons migrate via the external load to complete the circuit

$$S_x^{2-} + 2e \rightarrow S_{x-1}^{2-} + S^{2-} \quad (3)$$

Subsequently, photocurrent is generated in the QDSSC, win which the voltage is determined by variations in Fermi levels between the electron in the photoanode and the redox potential of $S^2\text{-}/S_x^{2-}$ in the electrolyte.

Fig. 7 schematic illustrates the energy diagram of Si QDSSC. As shown in Fig. 7, the work functions of ITO and Pt are -4.8 eV and -6.1 eV. The work function of FTO is -4.4 eV with respect to vacuum. The conduction band and valence band of TiO_2 are located at -4.33 eV and -7.53 eV, respectively. The conduction band and valence band of Si quantum dots are located at -4.05 eV and -5.8 eV, respectively, by assuming its bandgap of 2.2 eV. Consequently there is no potential barrier for excited electrons in Si quantum dots injecting into the TiO_2 film. In the other words, the high photocurrent can be resulted due to the vigorous electron supply from oxidized Si quantum dots to the TiO_2 photoanode as well from the electrolyte to oxidized Si quantum dots. The higher photocurrent in curve b demonstrates that the electron supply to Si quantum dots and the electron transfer of electrolyte are more efficient than those in curve a. On the other hand, open circuit voltage is determined by the difference between Fermi level of TiO_2 and redox potential of electrolyte, so no much difference in the open circuit voltage is observed for the two Si QDSSCs.

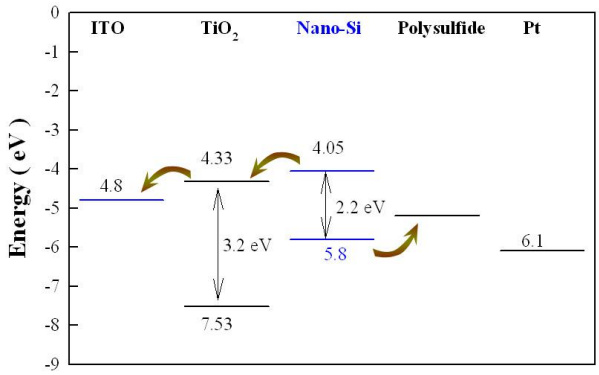

Fig. 7 Schematic illustration of the energy diagram of Si QDSSC..

Although there is no problem in the energy levels matching, the power conversion efficiency is extremely low for our Si QDSSCs. Some researchers proposed that charge recombination losses are primarily responsible for the low photovoltaic performance of QDSSCs. Charge recombination occurring at the photoanode/electrolyte interface contributes significant

energy loss in QDSSC devices. Another important reason for the low conversion efficiency of Si QDSSCs may be that Si quantum dots are easily oxidized to form an insulating SiO_2 layer at the surface of Si quantum dots. Fig. 8 represents the selected area electron diffraction of Si quantum dots to show the amorphous materials around Si quantum dots. It is clear that some portion of the Si quantum dot is amorphous. As discussed earlier in this paper, the outer shell of a Si quantum dot can be quickly oxidized into silicon dioxide once exposed in ambient air for a couple of minutes. The presence of SiO_2 layer acts as potential barrier which makes it more difficult for the excited electrons injected into TiO_2 film. Consequently, such a silicon dioxide layer deceases the photocurrent and leads to a rather low power conversion efficiency for Si QDSSCs.

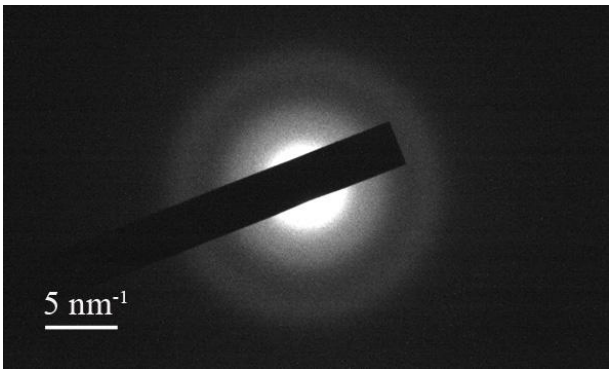

Fig. 8 Selected area electron diffraction of Si quantum dots.

4. Conclusions

This work is focused on Si QDSSC because of their toxicity and scarcity. The porous TiO_2 film is used as the backbone of the photoanode, and the structure of Si QDSSC is similar to that of dye-sensitized solar cell except the polysulfide electrolyte is used to substitute the conventional electrolyte I^-/I_3^- in order to match Si quantum dots. The *J-V* curve measurement has demonstrated that the power conversion efficiency of Si QDSSCs is as low as 0.052%. One possible reason is the formation of SiO_2 insulating layer at the surface of Si quantum dots. Our results suggest that Si quantum dots are not good candidates for QDSSCs. New kinds of quantum dots should be employed as the sensitizer so that QDSSCs can have a promising future.

Acknowledgment

This work was financially supported by Natural Science Foundation of China under the Grant No 11574036.

References

[1] M. Kouhnavard, S. Ikeda, N.A. Ludin, N.B.A. Khairudin, B.V. Ghaffari, M.A. Mat-Teridi, M.A. Ibrahim, S. Sepeai, K. Sopian. A review of semiconductor materials as sensitizers for quantum dot-sensitized solar cells. *Renew. Sust. Energ. Rev*. **37** (2014) 397-407.

[2] B. O'Regan, M. Grätzel. A low-cost, high-efficiency solar cell based on dye sensitized colloidal TiO_2 film. *Nature* **353** (1991) 737-740.

[3] L. Yang, Q.L. Ma, Y.G. Cai, Y.M. Huang. Enhanced photovoltaic performance of dye sensitized solar cells using one dimensional ZnO nanorod decorated porous TiO_2 film electrode. *Appl. Surf. Sci.* **292** (2014) 297-300.

[4] B.G. Zhai, L. Yang, Y.M. Huang. Improving the efficiency of dye-sensitized solar cells by growing longer ZnO nanorods on TiO_2 photoanodes. *J. Nanomater.* **2017** (2017) 1821837.

[5] B.G. Zhai, L. Yang, Y.M. Huang. ZnO nanorods decorated graphene/ZnO nanoparticle composite as the counter electrode of dye-sensitized solar cells. *Mater. Res. Innov.* **19** (2015) s15-s20.

[6] Q.L. Ma, Y.M. Huang. Improved photovoltaic performance of dye sensitized solar cell by decorating TiO_2 photoanode with Li-doped ZnO nanorods. *Mater. Lett.* **148** (2015) 171-173.

[7] L. Yang, B.G. Zhai, Q.L. Ma, Y.M. Huang. Effect of ZnO decoration on the photovoltaic performance of TiO_2 based dye sensitized solar cells. *J. Alloys Compd.* **605** (2014) 109-112.

[8] G.Z. Wu, Y. Shen, Q.S. Wu, F. Gu, M. Gao, L.J. Wang, Sol-modified ZnO photoanode for highly-efficient quantum dots sensitized solar cells. *J. Alloys Compd.* **551** (2013) 176-179.

[9] J. Jiao, Z.-J. Zhou, W.-H. Zhou, S.-X. Wu. CdS and PbS quantum dots co-sensitized TiO_2 nanorod arrays with improved performance for solar cells application. *Mater. Sci. Semicond. Process.* **16** (2013) 435-440.

[10] X.H. Song, M.Q. Wang, T.Y. Xing, J.P. Deng, J.J. Ding, Z. Yang, X.Y. Zhang. Fabrication of micro/nano-composite porous TiO_2 electrodes for quantum dot-sensitized solar cells. *J. Power Sources* **253** (2014) 17-26.

[11] C.J. Raj, S.N. Karthick, K.V. Hemalatha, H.-J. Kim, K. Prabakar, Highly efficient ZnO porous nanostructure for CdS/CdSe quantum dot sensitized solar cell. *Thin Solid Films* **548** (2013) 636-640.

[12] Y.M. Huang. Laser light scattering characterization of particle size distribution in porous silicon. *Solid State Commun.* **97** (1996) 33-37.

[13] Y.M. Huang. Photoluminescence of copper-doped porous silicon. *Appl. Phys. Lett.* **69** (1996) 3282-3284.

[14] Y.M. Huang. Positron irradiation: A technique for modifying the photoluminescent structures of porous silicon. *Appl. Phys. Lett.* **71** (1997) 3850-3852.

[15] A. Troia, A. Giovannozzi, G. Amato. Preparation of tunable silicon q-dots through ultrasound. *Ultrason. Sonochem.* **16** (2009) 448-451.

[16] H. Seo, Y.T. Wang, G. Uchida, K. Kamataki, N. Itagaki, K. Koga, M. Shiratani. Analysis on the effect of polysulfide electrolyte composition for higher performance of Si quantum dot-sensitized solar cells. *Electrochim. Acta* **95** (2013) 43-47.

[17] H. Seo, Y.T. Wang, G. Uchida, K. Kamataki, N. Itagaki, K. Koga, M. Shiratani, The optical analysis and application of size-controllable Si quantum dots fabricated by multi-hollow discharge plasma chemical vapor deposition. *Mater. Res. Soc. Symp. Proc.* **1426** (2012) 313-318.

[18] H. Seo, M.-K. Son, H.J. Kim, Y.T. Wang, G. Uchida, K. Kamataki, N. Itagaki, K. Koga, M. Shiratani, Study on the fabrication of paint-type Si quantum dot-sensitized solar cells. *Jpn. J. Appl. Phys.* **52** (2013) 10MB07.

[19] H. Kobayashi, P. Chewchinda, Y. Inoue, H. Funakubo, M. Hara, M. Fujino, O. Odawara, H. Wada, Photovoltaic properties of Si-based quantum-dot-sensitized solar cells prepared using laser plasma in liquid. *Jpn. J. Appl. Phys.* **53** (2014) 010208.

[20] H. Seo, Y.T. Wang, G. Uchida, K. Kamataki, N. Itagaki, K. Koga, M. Shiratani. The reduction of charge recombination and performance enhancement by the surface modification of Si quantum dot-sensitized solar cell. *Electrochim. Acta* **87** (2013)

213-217.

[21] H. Seo, Y.T. Wang, M. Sato, G. Uchida, K. Koga, N. Itagaki, K. Kamataki, M. Shiratani. The improvement on the performance of quantum dot-sensitized solar cells with functionalized Si. *Thin Solid Films* **546** (2013) 284-288.

[22] H. Seo, Y.T. Wang, M. Sato, G. Uchida, K. Kamataki, N. Itagaki, K. Koga, M. Shiratani. Improvement of Si adhesion and reduction of electron recombination for Si quantum dot-sensitized solar cells. *Jpn. J. Appl. Phys.* **52** (2013) 01AD05.

[23] Q.L. Ma, R. Xiong, Y.M. Huang. Tunable photoluminescence of porous silicon by liquid crystal infiltration. *J. Lumin.* **131** (2011) 2053-2057.

[24] Q.L. Ma, B.G. Zhai, Y.M. Huang, Sol-gel derived ZnO/porous silicon composites for tunable photoluminescence. *J. Sol-Gel Sci. Technol.* **64** (2012) 110-116.

[25] Y.M. Huang, B.G. Zhai, Q.L. Ma, L. Yang, Z.R. She. Anodization current density independent photoluminescence of porous silicon. *Key Eng. Mater.* **538** (2013) 85-88.

[26] Y.M. Huang and B.G. Zhai, Fourier transform infrared study of porous silicon dipped into Cr^{3+} solution. *J. Vac. Sci. Technol. B* **15** (1997) 1899-1901.